28. Spectroscopic Studies of Cyclometallated Pd(II) and Pt(II) Complexes: Optical Absorption and Emission of Single Crystals of [Pd(thpy)$_2$] and [Pt(thpy)$_2$]

by **Raimund Schwarz** and **Günter Gliemann***

Institut für Physikalische und Theoretische Chemie, Universität Regensburg, D-8400 Regensburg

and **Laurent Chassot, Philippe Jolliet,** and **Alex von Zelewsky***

Institute of Inorganic Chemistry, University of Fribourg, CH-1700 Fribourg

(7.X.88)

The polarized optical absorption and emission (spectra, decay times) of single crystals of [Pd(thpy)$_2$] and [Pt(thpy)$_2$] (thpy ≡ C(3′)-deprotonated form of 2-(2-thienyl)pyridine) at temperatures 1.9 K ≤ T ≤ 80 K are reported. The emission of [Pt(thpy)$_2$] can be influenced strongly by applied magnetic fields ($0 \leq H \leq 6$ T). Depending on the central ions Pd and Pt, the lowest excited electronic states of the single complexes are ligand-centered (LC) states and metal-to-ligand charge transfer (MLCT) states, respectively. This difference leads to distinctly dissimilar properties of the emission of both compounds. The experimental data show that the emission of single crystals of [Pd(thpy)$_2$] and [Pt(thpy)$_2$] at $T \leqslant 30$ K originates from several types of traps (defect states of symmetry $^3B_2$-stabilized below the exciton band) with LC and MLCT character, respectively. In the Pt compound, the $^3B_2$ is split by spin-orbit coupling into three states. The states B_1' and A_2', which determine the emission properties, are separated by $\Delta\bar{\nu} \sim 13\ cm^{-1}$. Both states can mix under the influence of an applied magnetic field yielding an increase of the emission intensity by a factor of ~ 1.5 at $H = 6$ T.

1. Introduction. – During recent years, several efforts have been made to understand the photochemistry, photophysics, and electrochemistry of cyclometallated transition-metal complexes, that can be employed as light-absorption sensitizers (LAS) and/or as light-emission sensitizers (LES) for the interconversion between light energy and chemical energy [1–9]. Most of the studies deal with cyclometallated homoleptic Pd(II) and Pt(II) complexes [5–9]. With regard to their optical properties (shape and energy of the absorption and emission bands, emission lifetime), they can be classified into two main types, corresponding to the character of the lowest excited electronic states: the Pd(II) complexes with excited ligand-centered (LC) states and the Pt(II) complexes with excited metal-to-ligand charge transfer (MLCT) states. All experiments and assignments mentioned above are restricted to solutions and/or glasses. Relatively little information is available on the optical properties of the crystal.

Recently, the polarized low temperature absorption and emission of single crystals of [Pd(bhq)$_2$] (Hbhq = benzo[*h*]quinoline) [10], [Pt(bhq)$_2$] [11], and [Pt(phpy)$_2$] (Hphpy = 2-phenylpyridine) [12] have been reported. From measurements at high magnetic fields, details of the electronic structure of these complexes could be established. The character of the low-energy optical transitions and the symmetry and energetic order of the emitting states have been assigned. To interpret the unusual temperature dependence of the emission spectra and decay times of single crystals of [Pd(bhq)$_2$] and [Pt(bhq)$_2$], energy-level diagrams have been developed, which consider the existence of traps located energe-

tically below the exciton bands [10] [11]. The spectroscopic properties of single crystal of $[Pt(phpy)_2]$ can be described by an energy-level diagram of oriented dimeric units of complexes.

In this paper, we present the results of our investigations on the optical properties of single crystals of $[Pd(thpy)_2]$ and $[Pt(thpy)_2]$ (thpy = C(3')-deprotonated form of 2-(2-thienyl)pyridine) as functions of temperature and applied magnetic fields. An important goal of this work is to analyse the experimental data and to compare the results with the qualitative models established for the other complexes mentioned above.

2. Experimental. – Single crystals of $[Pd(thpy)_2]$ and $[Pt(thpy)_2]$ were prepared by the methods described in [7] [8] [13]. The needle-shaped crystals of $[Pd(thpy)_2]$ used for the spectroscopic measurements had a typical size of $\sim 3 \times 0.1 \times 0.05$ mm^3. The orientation of the needle axis is denoted by **b**. It coincides with the crystallographic *b* axis. $[Pt(thpy)_2]$ formed rhombic crystals, whereas the shape of the rhombs varied from crystal to crystal. All $[Pt(thpy)_2]$ crystals exhibited double refraction under crossed polarizers with extinction parallel and perpendicular to one of the crystal axes, in the following denoted as **A**. The spectroscopic studies have been carried out with $[Pt(thpy)_2]$ crystals whose rhombic face had a size of $\sim 1 \times 1$ mm^2.

The measurements of the polarized absorption and emission spectra and of the emission lifetimes at different temperatures and at different magnetic field strengths have been performed using apparatus described in [14] [15]. For the emission measurements, the electric field vector of the exciting laser beam was parallel to the needle axis **b** for $[Pd(thpy)_2]$ and perpendicular to the axis **A** for $[Pt(thpy)_2]$, respectively.

3. Results. – 3.1. *[Pd(thpy)$_2$]. Fig. 1* shows the **E**$\|$**b** polarized absorption spectrum of single crystal of $[Pd(thpy)_2]$ at $T = 10$ K. **E** is the electric field vector of the light. The absorption band of lowest energy, labeled by *a*, has its maximum at $\tilde{\nu} = 18\,429$ cm^{-1} and a halfwidth of $\Delta\tilde{\nu} \approx 120$ cm^{-1}. Assuming that the molar concentration of $[Pd(thpy)_2]$ in the crystal equals that of $[Pt(bhq)_2]$, $c = 3.68$ mol/l [16], the extinction coefficient of this band is in the order of $\varepsilon \sim 30$ l · mol^{-1} · cm^{-1}. The absorption maxima *b*, *c*, and *d* are higher in

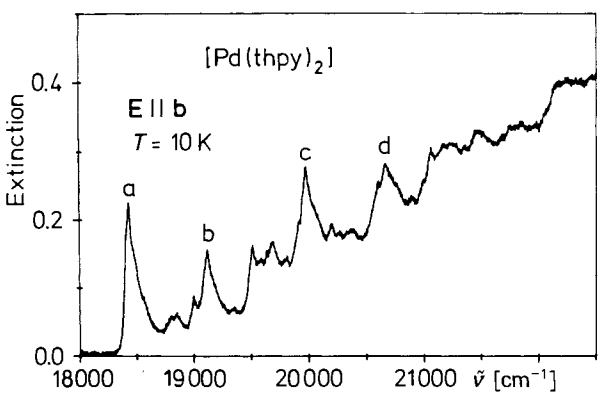

Fig. 1. **E**$\|$**b** *Polarized absorption spectrum of single crystal of [Pd(thpy)$_2$] at* T = *10 K.* Thickness of the crystals 20 μm.

energy than *a* by 695 cm^{-1}, 1560 cm^{-1}, and 2230 cm^{-1}, respectively. A common feature of the absorption bands *a*, *b*, *c*, and *d* is their asymmetrical shape. The **E** $\perp$ **b** polarized absorption spectrum does not differ at all from the **E**$\|$**b** spectrum, and the polarization ratio of the intensities is $I_\perp/I_\| = 1$. Raising the temperature from $T = 10$ K to room temperature, neither the band energies nor the intensities of the polarized absorption spectra are influenced.

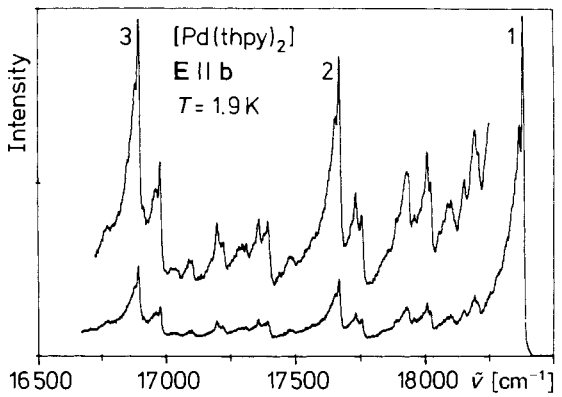

Fig. 2. **E**‖**b** *Polarized emission spectrum of single crystal of [Pd(thpy)$_2$] at* T = *1.9 K.* Expanded high-energy section. λ_{exc} = 364 nm.

Fig. 2 presents the high-energy section of the **E**‖**b** polarized emission spectrum at T = 1.9 K. The **E** ⊥ **b** polarized spectrum is very similar to this, especially concerning the band shapes, and the energies and intensities of the bands. As can be seen from *Fig. 2*, the structured spectrum is dominated by the three bands *1*, *2*, and *3*. Each of these bands is composed of one sharp high-energy peak showing no splitting within the limit of resolution ($\leq 2\ cm^{-1}$) and a broader one of lower intensity at its red flank. The peaks *2* and *3* are energetically separated from peak *1* by 708 cm^{-1} and 1481 cm^{-1}, respectively. It is conspicious that energies of the same order has been observed as the differences between

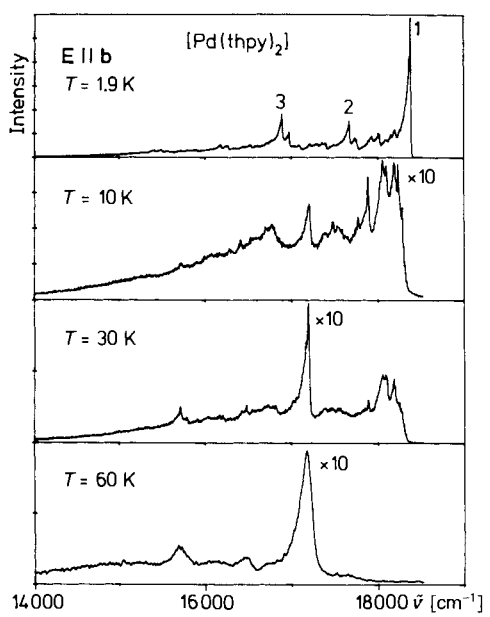

Fig. 3. **E**‖**b** *Polarized emission spectra of single crystal of [Pd(thpy)$_2$] at* T = *1.9 K, 10 K, 30 K, and 60 K.* λ_{exc} = 364 nm.

the absorption band *a* and the bands *b* and *c*, respectively. The emission peak *1* and the maximum of the absorption band *a* are separated by an energy gap of $\Delta\tilde{\nu} \approx 50\ cm^{-1}$.

Fig. 3 shows the influence of temperature on the **E**‖**b** polarized emission spectrum. Raising the temperature from $T = 1.9$ K to ~ 10 K, the sharp peaks *1*, *2*, and *3* vanish, and a spectrum with a distinctly different structure develops. Further increase of temperature to $T = 60$ K yields at first a fictitious red-shift of the emission and a smoothening of its structure, and finally an intensity breakdown at the high-energy section of the spectrum. The main maximum of the 60-K spectrum does not coincide with one of the peaks of the 1.9-K spectrum. Nevertheless the spectrum at $T = 60$ K has the same shape and coarse structure as the 1.9-K spectrum. Both spectra, however, are shifted against each other by $\Delta\tilde{\nu} \approx 1100\ cm^{-1}$.

Increasing temperature reduces the quantum yield. Between $T = 1.9$ K and ~ 30 K, the intensity ratio $I_\parallel/I_\perp$ is reduced by a factor of ~ 1.5, and at higher temperatures it remains constant within the limits of experimental error, *cf. Fig. 4*.

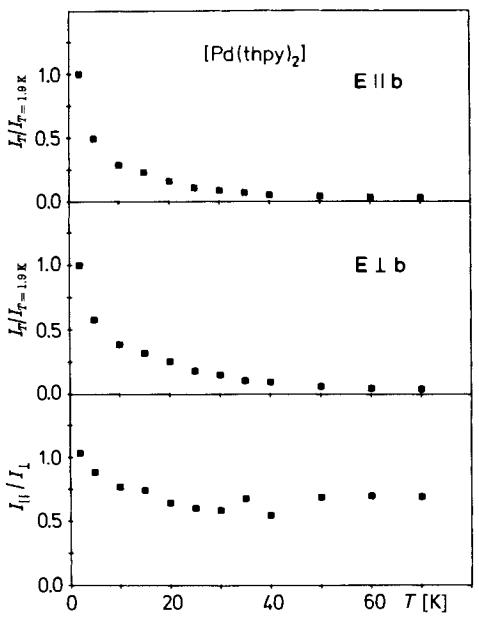

Fig. 4. *Relative emission intensity,* $I_T/I_{T=1.9\,K}$ *= 1.9 K, of the polarized emission of single crystal of [Pd(thpy)$_2$] as a function of temperature.* $\lambda_{exc} = 364$ nm.

At $T = 1.9$ K, the lifetime of the emission is $\tau = 85$ μs. This value is independent of the direction of polarization and of the wavelength of detection. At higher temperatures, the luminescence-decay curves are non-monoexponential, and they depend on the wavelength of detection. The lower the wavelength the faster is the luminescence decay. Thus, an intrinsic lifetime is not defined. Applied magnetic fields ($0 \leq H \leq 6$ T) do not affect the emission (spectra, decay times) of single crystal of [Pd(thpy)$_2$].

3.2. *[Pt(thpy)$_2$].* The spectrum of the **E** ⊥ **A** polarized emission of single crystal of [Pt(thpy)$_2$] (**A**: defined reference axis of the rhomb) shows at low temperature a structure

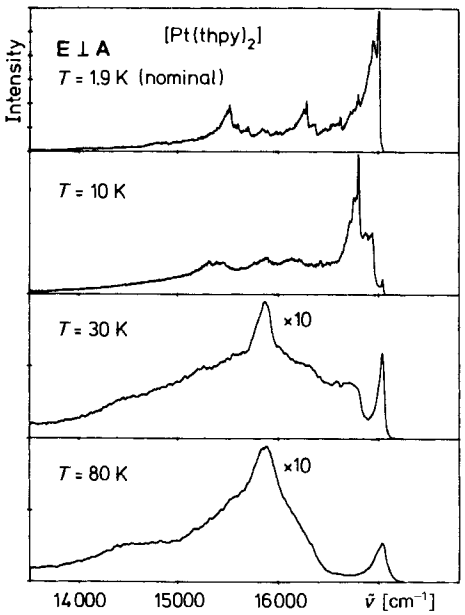

Fig. 5. **E** ⊥ **A** *Polarized emission spectra of single crystal of [Pt(thpy)$_2$] at* T = *1.9 K (nominal), 10 K, 30 K, and 80 K.* λ_{exc} = 364 nm.

which is very similar to that of the [Pd(thpy)$_2$] emission, *cf. Fig. 5*. As mentioned below *(cf. Chapt. 4.2.)*, for single crystal of [Pt(thpy)$_2$] the lowest temperature of the emitting crystal area is expected to be higher than the value $T = 1.9$ K measured in the sample chamber. Therefore, we denote the lowest temperature of the sample as $T = 1.9$ K (nominal). The main maximum of the emission has an energy of $\tilde{\nu} \approx 17000$ cm^{-1} followed by two weaker bands lower in energy by 708 cm^{-1} and 1480 cm^{-1}. In comparison with the emission spectrum of [Pd(thpy)$_2$], however, the spectrum of the Pt compound on the whole is shifted to lower energy by $\Delta\tilde{\nu} = 1380$ cm^{-1}.

The **E**∥**A** polarized emission spectrum coincides roughly with the **E** ⊥ **A** spectrum concerning the spectral position and the shape, but it is less intense by a factor of ~ 2. Between the two spectra, there exists a further important difference as shown in *Fig. 6*. The **E** ⊥ **A** polarized spectrum exhibits an intense peak denoted by *2*, which can be revealed only as a shoulder in the **E**∥**A** polarized spectrum. The energy separation between the peaks *1* and *2* amounts to $\Delta\tilde{\nu} = 13$ cm^{-1}. At the blue flanks of both emission spectra, two further peaks *3* and *4* at ~ 17024 cm^{-1} and ~ 17039 cm^{-1}, respectively, are resolved.

The temperature dependence of the **E** ⊥ **A** polarized emission spectrum is given in *Fig. 5*. Between $T = 1.9$ K (nominal) and 10 K, the high-energy part of the emission diminishes and, thus, a fictitious red-shift of the emission results. Further increase of the temperature induces no additional energy shift of the emission, but it smoothes the spectra. At temperatures $T \geqslant 30$ K, the spectra show a weak band at $\tilde{\nu} = 17040$ cm^{-1} and a broad intense one with maximum at ~ 15990 cm^{-1}. Temperature increase from $T =$ 1.9 K (nominal) to 60 K reduces the integral intensity of the emission, whereas the ratio of the intensities, $I_{\perp}/I_{\parallel} \approx 2$, remains constant, *cf. Fig. 7*.

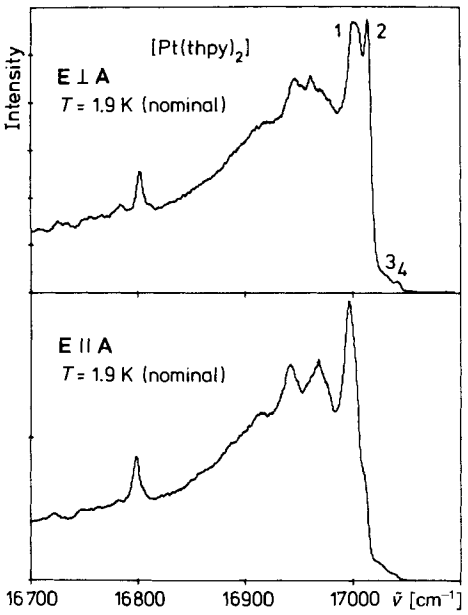

Fig. 6. *Expanded high-energy section of the polarized emission spectra of single crystal of [Pt(thpy)$_2$] at* T = *1.9 K (nominal).* λ_{exc} = 364 nm.

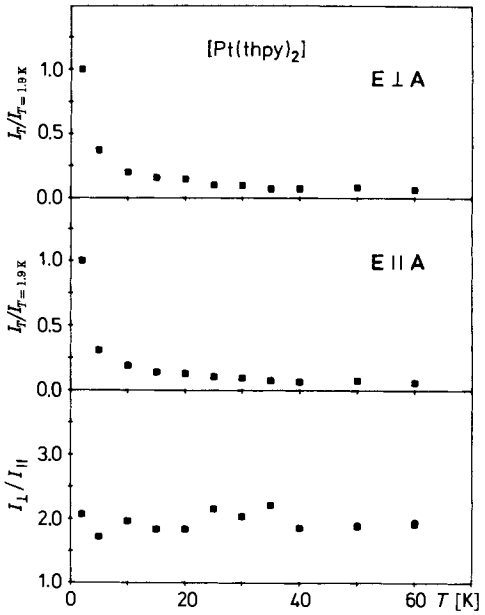

Fig. 7. *Relative emission intensity,* $I_T/I_{T=1.9\,K}$ = *1.9 K, of the polarized emission of single crystal of [Pt(thpy)$_2$] as a function of temperature.* λ_{exc} = 364 nm.

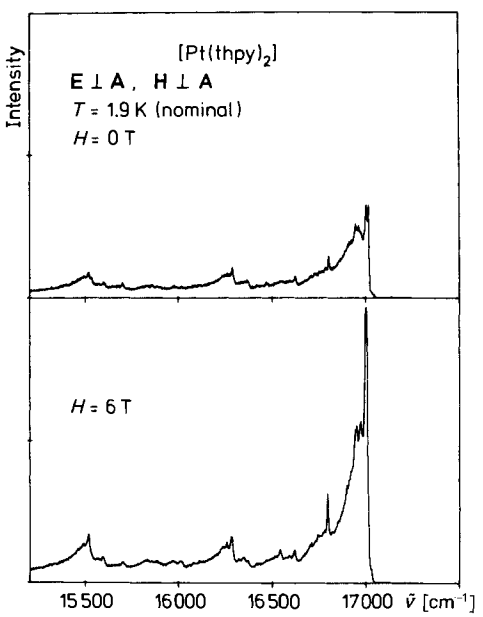

Fig. 8. **E** ⊥ **A** *Emission spectra of single crystal of [Pt(thpy)$_2$] at* H = *0 and 6* T. *T* = 1.9 K (nominal). λ_{exc} = 364 nm.

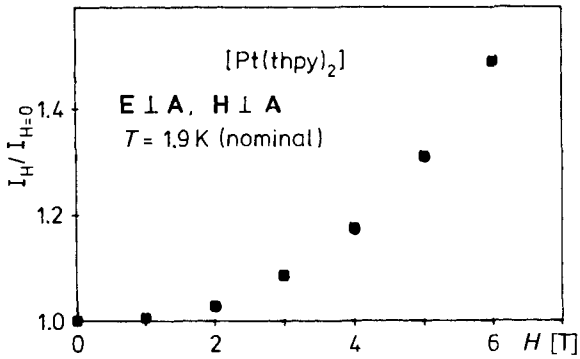

Fig. 9. *Relative emission intensity,* $I_H/I_H = 0$, *of the* $\mathbf{E} \perp \mathbf{A}$ *polarized emission of single crystal of* $[Pt(thpy)_2]$ *as a function of magnetic field strength* H *at* T = *1.9 K (nominal).* λ_{exc} = 364 nm.

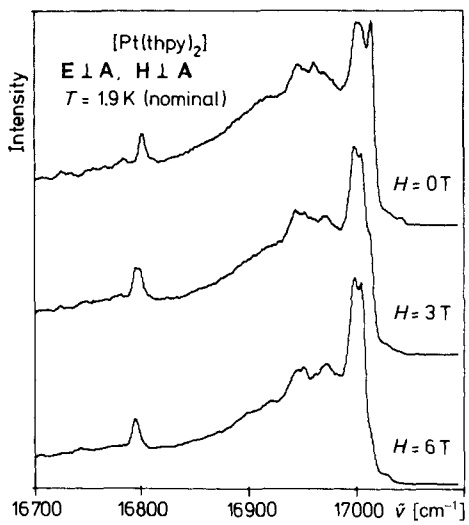

Fig. 10. *Expanded high-energy section of the* $\mathbf{E} \perp \mathbf{A}$ *polarized emission spectra of single crystal of* $[Pt(thpy)_2]$ *at* H = *0, 3 T and 6* T. *T* = 1.9 K (nominal). λ_{exc} = 364 nm.

The decay curves of the polarized emission at $T = 1.9$ K (nominal) vary weakly with the wavelength of detection and are not mono-exponential. For these reasons an intrinsic lifetime τ can not be specified. The long time slopes of the decay curves indicate for τ an upper limit of ~ 25 µs. At higher temperatures, the decay curves depend considerably on the wavelength of detection, and the behavior of the decay approachs that found for the Pd compound.

External magnetic fields $\mathbf{H} \perp \mathbf{A}$ strongly influence the $\mathbf{E} \perp \mathbf{A}$ emission spectrum, as shown in *Figs. 8–10.* At $T = 1.9$ K (nominal), the relative quantum yield $I_H/I_H = 0$ grows by a factor of ~ 1.5, if the field strength is raised from $H = 0$ to $H = 6$ *T,* and turns out to be a purely quadratic function of *H, cf. Figs. 8* and *9.* Furthermore, the magnetic field induces an intensity exchange between the peaks *2* and *1,* and between the peaks *4* and *3*

which are respectively separated by $\Delta\bar{\nu} \approx 13$ cm^{-1}. With increasing field strengths the peaks *2* and *4* lose intensity, whereas the intensity of the peaks *1* and *3* grows in, as presented in *Fig. 10*. Simultaneously, the peak at ~ 16800 cm^{-1} is red-shifted by $\Delta\bar{\nu} = 13$ cm^{-1}, if the field strength increases from $H = 0$ to $H = 6$ T, and moreover the shapes of the luminescence decay curves indicate increasing decay rates.

4. Discussion. – Until now, reports on the crystal structure of $[Pd(thpy)_2]$ and $[Pt(thpy)_2]$ are not available. The crystal structures of the related cyclometallated complexes $[Pt(bhq)_2]$ and $[Pt(Phpy)_2]$ [13], however, are well known. Because of the similarities of molecular structure, double refraction, and crystal morphology, the structure type of $[Pt(bhq)_2]$ is assumed to be valid also for the $[Pd(thpy)_2]$ crystal. The crystallographic *b* axis is parallel to the molecular *x* axis, *cf. Fig. 11*. The $[Pt(thpy)_2]$ crystals show no needle shape, however, as will be shown below, the experimental results are compatible with a formal substitution of $\mathbf{E} \perp \mathbf{A}$ by $\mathbf{E} \| \mathbf{b}$ and *vice versa*. Thus, in the following discussion the axis **A** is assumed to be perpendicular to the molecular *x* axis, although the experimental results indicate a small mixture of the different polarizations, *cf.* peak *2* in *Fig. 6*.

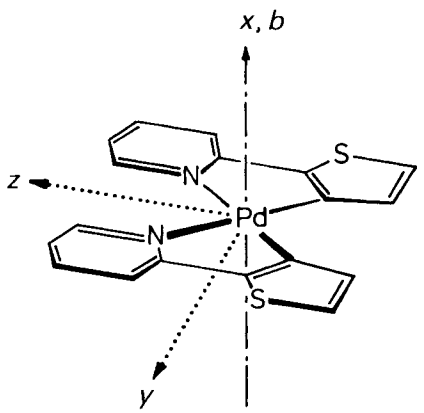

Fig. 11. *Schematic representation of the complex [Pd(thpy)$_2$]. x, y,* and *z* denote the molecular axes, *b* the crystallographic *b* axis.

To explain the observed effects, the local symmetry of the central metals can be described approximately by the point group C_{2v} (double group C'_{2v}).

As has been analysed for Pd(II) and Pt(II) complexes with aromatic C,N ligands, the LUMOs of the single complexes are stabilized ligand hybrid MOs of symmetry $b_1(\pi_L^*)$ [10] [11] [17] [18]. The HOMOs of the Pt compounds are destabilized metal states d_{xy} with a small admixture of ligand states π_L, $a_2(xy,\pi_L)$, whereas the HOMOs of the Pd compounds can be assigned to ligand MOs π_L with a small metal component d_{xy}, $a_2(\pi_L,xy)$. Thus, both types of complexes have the electronic ground state $^1A_1$ and from their first excited configuration ($a_2 \rightarrow b_1$) the terms $^1B_2$ and $^3B_2$ result, with $^3B_2$ the energetically lowest excited term. In spite of the same symmetry, the lowest excited states of $[Pt(thpy)_2]$ have predominantly MLCT character, while the lowest excited states of $[Pd(thpy)_2]$ are centered mainly at the ligands [9]. The characters of the lowest excited states of both systems, however,

differ only by the amount of mixing of d_{xy} and π_L. Accordingly, the spin-orbit coupling yields different effects for the two complexes. For the excited states of [Pd(thpy)$_2$], mainly an external spin-orbit coupling is expected, yielding an increase of the intersystem crossing rates but not an appreciable removal of the $^2B_2$ degeneracy. Because of the relatively strong internal spin-orbit coupling in the Pt complex, besides an intensification of the intersystem crossing rates an energetically considerable splitting of the $^3B_2$ results.

In the crystal, the excited states of the complexes form exciton bands. *Figs. 12* and *13* show corresponding energy-level diagrams originally developed for single crystals of [Pd(bhq)$_2$] and [Pt(bhq)$_2$] [10] [11]. For the interpretation of the observed optical properties, we assume the existence of X traps with sharp energy levels. The traps are due to complexes, which are disturbed by impurities or lattice defects. For sake of clearness, in *Figs. 12* and *13* only two different types of X traps are presented, a shallow X trap S stabilized by the energy ΔE_s and a deep X trap D with stabilization energy ΔE_d.

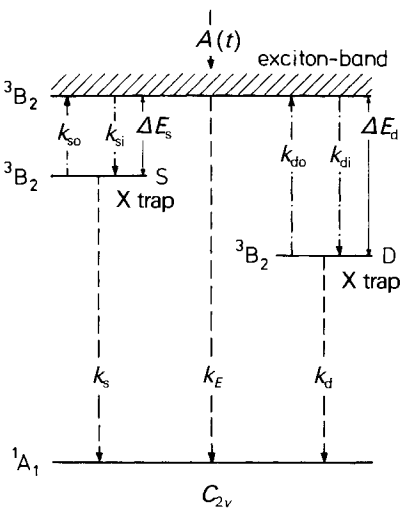

Fig. 12. *Proposed energy-level diagram of the lowest electronic states of single crystal of [Pd(thpy)$_2$].* S: shallow trap. D: deep trap.

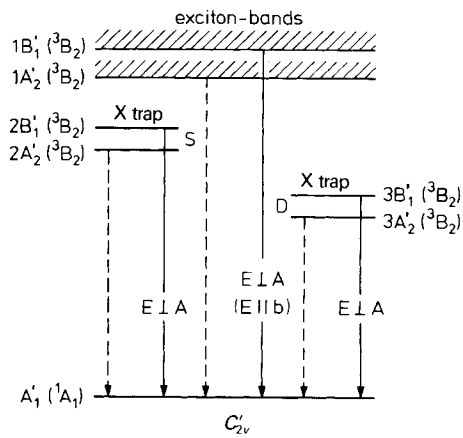

Fig. 13. *Proposed energy-level diagram of the lowest electronic states of single crystal of [Pt(thpy)$_2$].* S: shallow trap. D: deep trap.

4.1. *[Pd(thpy)$_2$].* The low-energy absorption band *a, cf. Fig. 1,* belongs to the spin-forbidden transition from the ground state $^1A_1$ to the $^3B_2$ exciton band, *cf. Fig. 12.* The relatively high value of the extinction coefficient, $\varepsilon \approx 30\ l \cdot mol^{-1} \cdot cm^{-1}$, is probably due to a weakening of the spin-selection rule by the external spin-orbit coupling *via* an admixture of metal state $a_2(xy)$ to the HOMO of the complex. The absorption bands *b, c,* and *d* are assigned to vibronic transitions which involve mainly molecular vibrations of the thpy heterocycle. This assignment follows from the occurrence of comparable vibration quanta in the absorption and/or emission spectra of both complexes, [Pd(thpy)$_2$] and [Pt(thpy)$_2$], being independent of the central ion. X-Trap absorption cannot be observed in the transmission spectra, because of the low concentration of the defect states.

The properties of the emission can be traced back to the radiative deactivation of the different types of X-traps, *cf. Fig. 12*. A radiationless relaxation of rate $A(t)$ populates the $^3B_2$ exciton band. The energy propagates rapidly within the exciton band and can be trapped by the defect states, with trapping rates $k_{si}, k_{di} \gg k_E$, *cf. Fig. 12*. A low trap concentration implies a large spatial separation of the traps. This precludes a direct energy transfer between the defect states by a *Förster-Dexter* mechanism. Therefore, the energy transfer is expected to proceed *via* the exciton band. At $T = 1.9$ K such thermal activated routes have a low probability and, therefore, no energy transfer between the traps will occur. Consequently, the emission at $T = 1.9$ K is the superposition of the luminescence of all types of X traps.

An application of model calculations concerning the transfer of excitation energy in organic single crystals [19–23] to the energy level diagram of single crystal [Pd(thpy)$_2$] shows that shallow X traps of one type, stabilized by $\Delta E_s \approx 50$ cm^{-1}, represent the majority of traps and these dominate the emission at $T = 1.9$ K. The peak *1* is assigned to the 0–0 transition of this type of trap, the peaks *2* and *3* are accompanying vibrational satellites, *cf. Fig. 2*. The splitting of the peaks *1, 2,* and *3* is caused probably by a phonon progression coupled to the electronic and vibronic transitions. The observed emission lifetime $\tau = 85$ µs of single crystal [Pd(thpy)$_2$] at $T = 1.9$ K is distinctly smaller than the value $\tau = 250$ µs found for [Pd(thpy)$_2$] dissolved in glasses at $T = 77$ K [9] and 1.9 K [24]. This difference is possibly due to an intercomplex coupling in the crystal.

With increasing temperature, the X traps can be depopulated by thermal activation into the exciton band with rates k_{so} and k_{do} according to their trap depths ΔE_s and ΔE_d, respectively [19–23]. At $T \approx 10$ K, only the shallow traps with $\Delta E_s \approx 50$ cm^{-1} are deactivated ($k_{so} \neq 0$, $k_{do} = 0$), and the corresponding peaks *1, 2,* and *3* of the emission spectra vanish, *cf. Fig. 3*. With further increase of temperature to $T = 60$ K, all traps, with exception of the deepest one ($\Delta E_d = 1100$ cm^{-1}), can be thermally activated into the exciton band, and, thus, only the deepest traps are occupied appreciably and yield the luminescence.

The assumption that the X traps originate from disturbed [Pd(thpy)$_2$] complexes is compatible with the observed characteristic dependence of the emission lifetime on the detection wavelength and the loss of the mono-exponential character of the decay curves at $T > 1.9$ K. The observed decrease of the integral emission quantum yield with increasing temperature, *cf. Fig. 4*, can be explained by a temperature-dependent non-radiative deactivation of the X traps and of the exciton band.

4.2. *[Pt(thpy)$_2$]*. The interpretation of the experimental results for single-crystal of [Pt(thpy)$_2$] can be based on the energy-level diagram shown in *Fig. 13*. It follows from the diagram for single crystal of [Pd(thpy)$_2$] *(Fig. 12)* by taking into account the effects of a relatively strong spin-orbit coupling. The increase of spin-orbit coupling is due to the larger ζ value of Pt and to the metal character of the $^3B_2$ term in the [Pt(thpy)$_2$] complex. By spin-orbit coupling, the term $^3B_2$ splits into the components A_1', A_2', and B_1'. As will be shown below, our experimental results can be explained, if these components have the energetic order of $A_2' < B_1' < A_1'$. The electronic ground state $^1A_1$ transforms in the double group C_{2v}' as A_1'. Transitions $B_1' \leftrightarrow A_1'$ are electric dipole allowed with polarization $\mathbf{E} \perp \mathbf{A}(\mathbf{E} \| \mathbf{b})$, while transitions $A_2' \leftrightarrow A_1'$ are forbidden. The disturbed complexes yielding the traps are expected to have a symmetry lower than C_{2v}. At this lower symmetry, the state

$A_2'(^3B_2)$ can mix with other excited states and, thus, the transitions $A_2'(^3B_2) \rightarrow A_1'(^1A_1)$ become radiatively allowed, possibly without any polarization.

Similar to the explanation of the luminescence of the Pd(II) complex, the luminescence of single crystal of $[Pt(thpy)_2]$ is expected to originate from a radiative deactivation of X traps. At $T = 1.9$ K (nominal), the most intense luminescence at $\tilde{\nu} = 17000$ cm^{-1} is dominated by one type of shallow X traps, *cf. Fig. 5*. The non-polarized emission peak, denoted by *1* in *Fig. 6*, belongs to the 0–0 transition $A_2'(^3B_2) \rightarrow A_1'(^1A_1)$. According to the selection rules the $\mathbf{E} \perp \mathbf{A}(\mathbf{E} \| \mathbf{b})$, polarized peak *2* is assigned to the allowed electric dipole transition from the excited state $B_1'(^3B_2)$ of the same trap to the ground state $A_1'(^1A_1)$. The energy difference of $\Delta\tilde{\nu} = 13$ cm^{-1} between the peaks *1* and *2* equals the energy separation of the spin-orbit components $A_2'(^3B_2)$ and $B_1'(^3B_2)$. Beside the X traps described above, a further type of X traps can be identified. The peaks *3* and *4* ($\tilde{\nu} = 17024$ cm^{-1}) correspond to a radiative deactivation of the states $A_2'(^3B_2)$ and $B_1'(^3B_2)$ of these traps, *cf. Fig. 6*.

The substitution of Pd by Pt in the $[Pd(thpy)_2]$ complex shortens the emission lifetime from $\tau = 85$ µs to ≈ 25 µs. This is in agreement with the MLCT character of the corresponding excited states in the Pt(II) complex and the relatively strong spin-orbit coupling in Pt.

The lowest excited states of a disturbed complex are $A_2'(^3B_2)$ and $B_1'(^3B_2)$ with an energy distance of $\Delta\tilde{\nu} = 13$ cm^{-1}. At $T = 1.9$ K, only the state $A_2'(^3B_2)$ should be populated appreciably. Nevertheless, also the luminescence from state $B_1'(^3B_2)$ can be observed in the $\mathbf{E} \perp \mathbf{A}$ polarized emission spectrum at $T = 1.9$ K (nominal), *cf. Fig. 6*. We are forced to assume that the exciting laser beam has heated the illuminated crystal surface, which represents the luminescent area, to a temperature distinctly higher than that of the sample chamber. Because of the low quantum yield of single crystal of $[Pt(thpy)_2]$ compared to the systems $[Pd(thpy)_2]$, $[Pd(bhq)_2]$, and $[Pt(bhq)_2]$ a distinctly higher laser power had to be applied for the excitation of $[Pt(thpy)_2]$. To reconcile the experimental results with the results found for single crystal of $[Pt(bhq)_2]$ [11], we estimate that the nominal value $T = 1.9$ K in reality corresponds to a temperature of ~ 5–10 K. This assumption is confirmed by the wavelength dependence and the non-monoexponential character of the decay for $[Pt(thpy)_2]$ at $T = 1.9$ K (nominal). The same effects have been observed for $[Pd(thpy)_2]$, $[Pd(bhq)_2]$, and $[Pt(bhy)_2]$ only at $T > 1.9$ K.

Raising the temperature, the different traps become depopulated one by one *via* the exciton band, corresponding to their depths. The spectra at $T > 30$ K indicate, that no traps exist, which are sufficiently deep to capture the excitation energy at higher temperatures. For this reason, the band of highest energy (maximum at $\tilde{\nu} = 17040$ cm^{-1}) of the 60-K emission spectrum is assigned to the radiative transitions from the exciton bands $A_2'(^3B_2)$ and/or $B_1'(^3B_2)$ to the ground state. From the corresponding peak energies, the depths of traps yielding the peaks *1, 2,* and *3, 4* in the emission spectra *(Fig. 6)* can be calculated as $\Delta\tilde{\nu} = 40$ cm^{-1} and 16 cm^{-1}, respectively.

For $[Pt(thpy)_2]$, the behavior of the decay rates and the emission intensities as functions of temperature can be explained in the same way as for $[Pd(thpy)_2]$.

Application of a homogeneous magnetic field $\mathbf{H} \perp \mathbf{A}$ $(\mathbf{H} \| \mathbf{b})$ lowers the C_{2v} symmetry of the complexes to C_s symmetry. The corresponding energy-level diagram and the selection rules for electric dipole transitions are shown in *Fig. 14*. At C_s symmetry, the spin-orbit states $A_2'(^3B_2)$ and $B_1'(^3B_2)$ can mix. Thus, an additional radiative channel with polarization $\mathbf{E} \perp \mathbf{A}(\mathbf{E} \| \mathbf{b})$ from the states $A_2'(^3B_2)$ to the ground state is opened. Since, with increasing

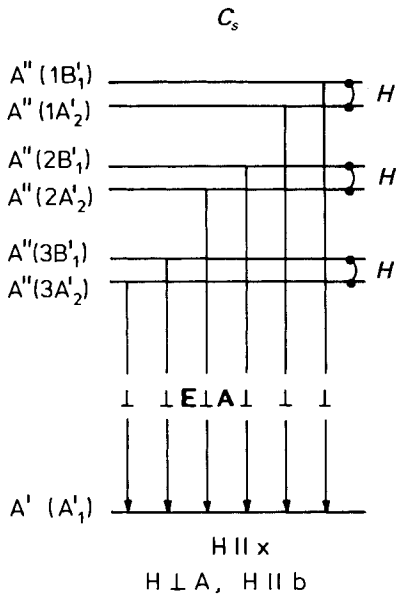

Fig. 14. *Proposed energy-level diagram of the lowest electronic states of single crystal of [Pt(thpy)$_2$] under the influence of a homogeneous magnetic field* **H** ⊥ **A** (**H**∥**x**, **b**)

field-strength H, the mixing of the states grows, the additional **E** ⊥ **A** polarized emission becomes more and more intense. The experimental result $I_{\perp,H} \approx H^2$, *cf. Figs. 8* and *9*, and the magnetic field induced increase of the luminescence decay rates corrobate the proposed model as can be shown by quantum mechanical perturbation theory [25–27]. The exchange of intensity within the pairs of peaks *1, 2,* and *3, 4,* as shown in *Fig. 10,* is caused by a *Zeeman* repulsion of the corresponding states $A_2'(^3B_2)$ and $B_1'(^3B_2)$, and by the magnetic-field-induced rate increase of the luminescence decay of the defects states $A_2'(^3B_2)$. The simultaneous red-shift ($\Delta\bar{\nu} = 13$ cm^{-1}) of the vibrational peak at $\bar{\nu} \approx 16800$ cm^{-1}, *cf. Fig. 10,* indicates that identical vibrations (same energy, same symmetry) are coupled to the excited spin-orbit states $A_2'(^3B_2)$ and $B_1'(^3B_2)$.

This research has been supported by the *Deutsche Forschungsgemeinschaft,* the *Fonds der Chemischen Industrie,* and the *Swiss National Science Foundation.*

REFERENCES

[1] S. Sprouse, K. A. King, R. J. Watts, *J. Am. Chem. Soc.* **1984,** *106,* 6647.
[2] Y. Ohsawa, S. Sprouse, K. A. King, M. K. DeArmond, K. W. Hank, R. J. Watts, *J. Phys. Chem.* **1987,** *91,* 1047.
[3] M. Maestri, D. Sandrini, V. Balzani, U. Maeder, A. v. Zelewsky, *Inorg. Chem.* **1987,** *26,* 1323.
[4] U. Maeder, T. Jenny, A. v. Zelewsky, *Helv. Chim. Acta* **1986,** *69,* 1085.
[5] M. Maestri, D. Sandrini, V. Balzani, L. Chassot, P. Jolliet, A. v. Zelewsky, *Chem. Phys. Lett.* **1985,** *122,* 375.
[6] S. Bonafede, M. Ciano, F. Bolletta, V. Balzani, L. Chassot, A. v. Zelewsky, *J. Phys. Chem.* **1986,** *90,* 3836.
[7] L. Chassot, A. v. Zelewsky, *Inorg. Chem.* **1987,** *26,* 2814.
[8] C. Cornioley-Deuschel, A. v. Zelewsky, *Inorg. Chem.* **1987,** *26,* 3354.

[9] M. Maestri, D. Sandrini, V. Balzani, A. v. Zelewsky, P. Jolliet, *Helv. Chim. Acta* **1988,** *71,* 134; V. Balzani, M. Maestri, A. Melandri, D. Sandrini, L. Chassot, C. Cornioley-Deuschel, P. Jolliet, U. Maeder, A. v. Zelewsky, '7th Int. Symp. on the Photochem. and Photophys. of Coord. Compounds', Elmau, Eds. H. Yersin and A. Vogler, Springer-Verlag, Heidelberg–New York, 1987.
[10] R. Schwarz, G. Gliemann, Ph. Jolliet, A. v. Zelewsky, submitted to *Inorg. Chem.*
[11] R. Schwarz, G. Gliemann, Ph. Jolliet, A. v. Zelewsky, submitted to *Inorg. Chem.*
[12] L. Bär, G. Gliemann, L. Chassot, A. v. Zelewsky, *Chem. Phys. Lett.* **1986,** *123,* 264.
[13] L. Chassot, E. Müller, A. v. Zelewsky, *Inorg. Chem.* **1984,** *23,* 4249.
[14] W. v. Ammon, Thesis, Universität Regensburg, 1981.
[15] W. Tuszynski, G. Gliemann, *Ber. Bunsenges. Phys. Chem.* **1985,** *89,* 940.
[16] G. Bernardinelli, A. v. Zelewsky, to be published.
[17] R. Schwarz, M. Lindner, G. Gliemann, *Ber. Bunsenges. Phys. Chem.* **1987,** *91,* 1233.
[18] J. Biedermann, M. Wallfahrer, G. Gliemann, *J. Luminesc.* **1987,** *37,* 323.
[19] M.D. Fayer, C.B. Harris, *Phys. Rev.* **1974,** *9,* 748.
[20] R.M. Shelby, A.H. Zewail, C.B. Harris, *J. Chem. Phys.* **1976,** *64,* 3192.
[21] W. Güttler, J.U. v. Schütz, H.C. Wolf, *Chem. Phys.* **1977,** *24,* 159.
[22] G. Weinzierl, J. Friedrich, *Chem. Phys. Lett.* **1981,** *83,* 204.
[23] M. Vala, J. Baiardo, A. Wierzbicki, I. Trabjerg, *Chem. Phys.* **1987,** *116,* 221.
[24] R. Schwarz, G. Gliemann, unpublished results.
[25] G. Gliemann, *Comments Inorg. Chem.* **1986,** *5,* 263.
[26] G. Gliemann, *Pure Appl. Chem.,* in press.
[27] G. Gliemann, H. Yersin, 'Structure and Bonding, 62', Springer-Verlag, Berlin–Heidelberg–New York, 1985.